Cell

Global Regulation of Promoter Melting in Naive Lymphocytes

Fedor Kouzine,[1,9] Damian Wojtowicz,[2,6,9] Arito Yamane,[3,9,10] Wolfgang Resch,[3] Kyong-Rim Kieffer-Kwon,[3] Russell Bandle,[1] Steevenson Nelson,[3] Hirotaka Nakahashi,[3] Parirokh Awasthi,[5] Lionel Feigenbaum,[5] Herve Menoni,[7] Jan Hoeijmakers,[7] Wim Vermeulen,[7] Hui Ge,[8] Teresa M. Przytycka,[2,9] David Levens,[1,9,*] and Rafael Casellas[3,4,9,*]
[1]Laboratory of Pathology, Center for Cancer Research, NCI
[2]National Center for Biotechnology Information, NLM
[3]Genomics and Immunity, NIAMS
[4]Center of Cancer Research, NCI
[5]Science Applications International Corporation, NCI
National Institutes of Health, Bethesda, MD 20892, USA
[6]Institute of Informatics, University of Warsaw, 02-098 Warsaw, Poland
[7]Department of Genetics, Biomedical Science, Erasmus Medical Center, 3015 GE Rotterdam, the Netherlands
[8]Ascentgene, Inc., Rockville, MD 20850, USA
[9]These authors contributed equally to this work
[10]Present address: Department of Molecular Pharmacology and Oncology, Gunma University Graduate School of Medicine, Maebashi, Gunma 371-8511, Japan
*Correspondence: levens@helix.nih.gov (D.L.), casellar@mail.nih.gov (R.C.)
http://dx.doi.org/10.1016/j.cell.2013.04.033

SUMMARY

Lymphocyte activation is initiated by a global increase in messenger RNA synthesis. However, the mechanisms driving transcriptome amplification during the immune response are unknown. By monitoring single-stranded DNA genome wide, we show that the genome of naive cells is poised for rapid activation. In G_0, ~90% of promoters from genes to be expressed in cycling lymphocytes are polymerase loaded but unmelted and support only basal transcription. Furthermore, the transition from abortive to productive elongation is kinetically limiting, causing polymerases to accumulate nearer to transcription start sites. Resting lymphocytes also limit the expression of the transcription factor IIH complex, including XPB and XPD helicases involved in promoter melting and open complex extension. To date, two rate-limiting steps have been shown to control global gene expression in eukaryotes: preinitiation complex assembly and polymerase pausing. Our studies identify promoter melting as a third key regulatory step and propose that this mechanism ensures a prompt lymphocyte response to invading pathogens.

INTRODUCTION

After active proliferation during bone marrow and thymic development, B and T cells rearrange their antigen receptors and migrate to the periphery as quiescent G_0 lymphocytes. Under these conditions, RNA and protein synthesis is maintained at basal levels, and energy output is limited (Sprent, 1993). However, upon contact with antigens in the periphery, resting lymphocytes drastically increase messenger RNA (mRNA) production, undergo cell division, and differentiate into short-lived effector or long-lived memory cells (Rajewsky, 1996). Thus, a successful adaptive immune response depends at least in part on a rapid shift from basal to fully activated gene expression. However, the molecular mechanisms controlling transcriptome amplification have not been defined.

Eukaryotic gene expression is driven by a complex series of ordered events, including RNA polymerase II (PolII) recruitment, preinitiation complex assembly, open complex formation, promoter escape, pausing, elongation, and transcriptional termination (Fuda et al., 2009; Lee and Young, 2000; Orphanides and Reinberg, 2000). Until recently, it was generally believed that the expression of most protein-coding genes was regulated at the level of holoenzyme recruitment to promoter regions (Margaritis and Holstege, 2008; Ptashne and Gann, 1997; Roeder, 2005). Potential exceptions to this rule were the *Drosophila* heat shock (Gilmour and Lis, 1986) and a small number of human genes, including *MYC* (Bentley and Groudine, 1986), which display PolII pausing downstream of the transcription start site (TSS). In such cases, transcriptional regulation was proposed to occur by controlling the rate of PolII pause release. However, subsequent genome-wide surveys revealed PolII accumulation at the vast majority of transcriptionally active promoters (Core et al., 2008; Kim et al., 2005; Muse et al., 2007; Rahl et al., 2010; Seila et al., 2009; Zeitlinger et al., 2007), indicating that the rate of pause release might, in fact, be limiting across the genome. In addition to active sites, a fraction of unexpressed genes were also associated with paused polymerases and displayed the hallmarks of transcription initiation without elongation

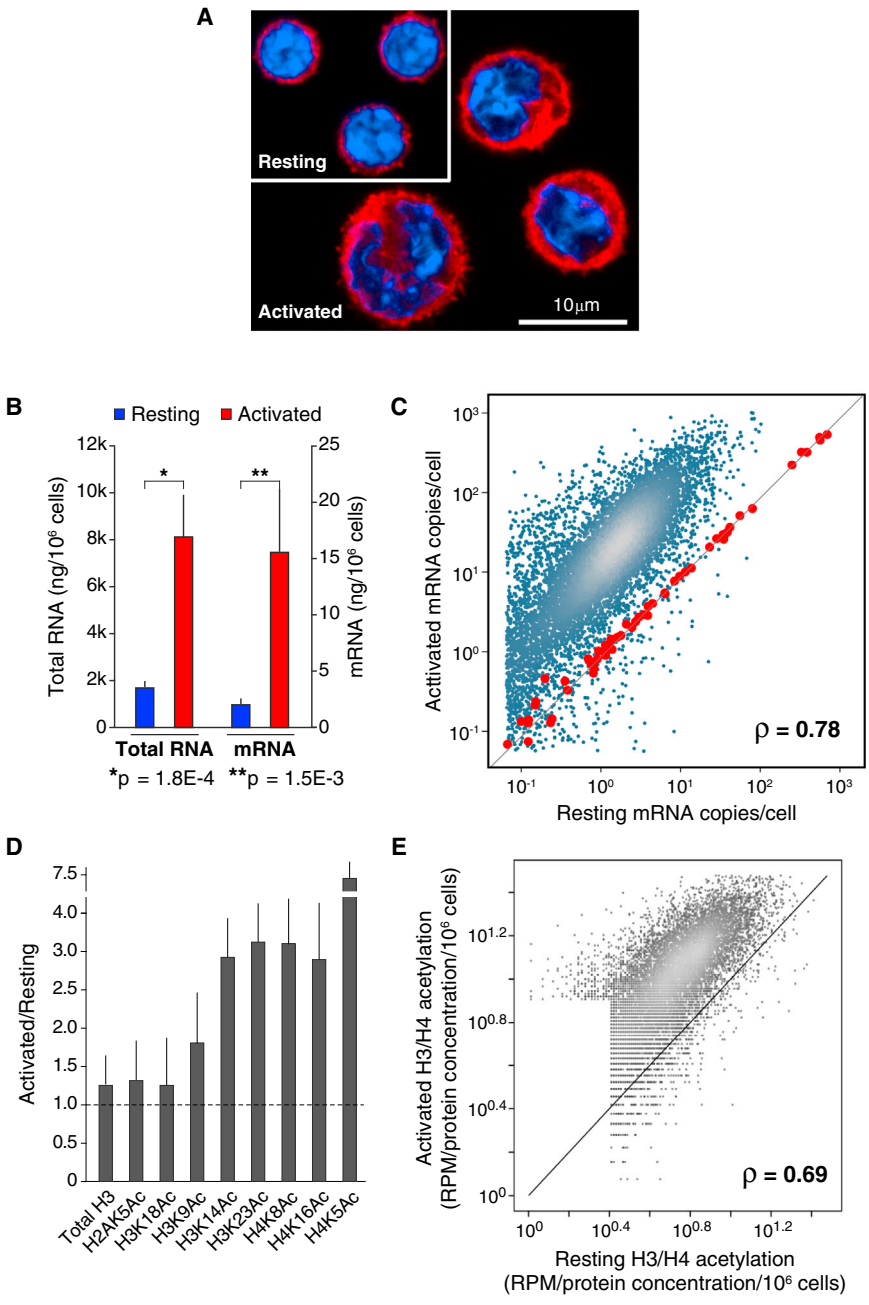

Figure 1. Proportional Upregulation of mRNA Synthesis and Histone Acetylation during B Cell Activation

(A) Confocal micrograph showing representative examples of resting (G_0) and activated (cycling plasmacytes) B cells. Samples were stained with anti-α-tubulin (red) and DAPI (blue).

(B) Bar graph portraying total RNA (isolated with TRIzol reagent) and mRNA (isolated with oligo [dT] microbeads) from resting (blue bars) and activated (red bars) B lymphocytes (measured as ng/10^6 cells). Data represent the mean values ± SEM; n = 4 for all samples.

(C) Comparison of resting and activated B cell transcriptomes, as determined by mRNA-seq analysis. Values represent mRNA copies per cell and were calculated on the basis of mRNA standards (red dots) spiked-in to total RNA isolated from 10^6 resting or activated B cells.

(D) Reverse phase protein microarray analysis of histones H3 and H4 lysine acetylation marks during B cell activation. Bars represent the ratio of total acetylation measured in activated versus naive cells. Total histone H3 was used as "loading" control.

(E) Comparison of histone H3 (K14 and K23) and H4 (K5, K8, and K16) acetylation in resting and activated B cells as measured by ChIP-seq and normalized with RPMA values. Correlation in (C) and (E) was calculated via Spearman's ρ test. See also Table S1.

RESULTS

A Proportional Increase in mRNA Synthesis and Histone Acetylation upon Lymphocyte Activation

To explore transcriptional regulation during lymphocyte activation, we stimulated naive CD43$^-$ mouse splenic B cells in the presence of lipopolysaccharide and interleukin 4 (LPS+IL4) ex vivo. These conditions promote a drastic increase in cell size, proliferation, and plasma cell terminal differentiation (Rajewsky, 1996; Shapiro-Shelef and Calame, 2005) (Figure 1A). These morphological changes are preceded in the nucleus by global chromatin decondensation, enhanced histone acetylation, and gene activation (Fisher, 2005; Melchers and Andersson, 1984; Pogo et al., 1966, 1967; Rawlings et al., 2011). In agreement with this view, we observed a nearly 10-fold increase in total RNA and mRNA production, given that resting B cells differentiated for 48 hr in the presence of LPS+IL4 ($p < 1.5 \times 10^{-3}$; Figure 1B).

Enhanced mRNA synthesis during activation might result from the de novo transcription of a subset of genes. Alternatively, naive lymphocytes may upregulate the expression of most genes as they enter the cell cycle, a process known as transcriptome amplification (Lin et al., 2012; Lovén et al., 2012; Nie et al., (Bernstein et al., 2006; Guenther et al., 2007; Lee et al., 2006; Radonjic et al., 2005; Yamane et al., 2011).

Thus, the aforementioned studies have provided the basis for our current view that both holoenzyme recruitment and polymerase pausing are key rate-limiting steps in eukaryote gene expression. However, it is important to point out that, to date, genome-wide transcription studies have been by and large limited to cycling cells. By means of a protocol we developed that maps single-stranded DNA (ssDNA) across the genome, we show that noncycling, G_0 lymphocytes use promoter melting as an additional step to globally regulate transcription in eukaryotes.

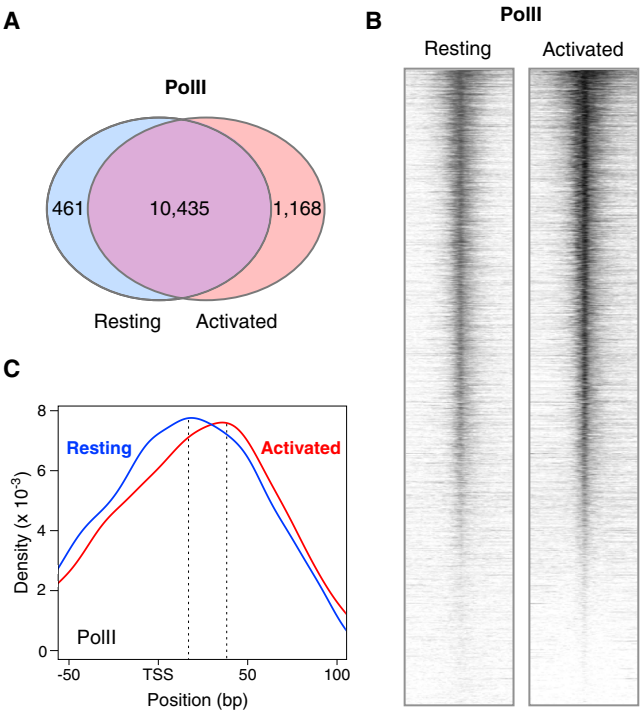

Figure 2. PolII Recruitment and Promoter Profiles during B Cell Activation

(A) Venn diagram showing the number of genes in resting (blue circle) and stimulated (red circle) B cells that are associated with PolII ChIP-seq signals.

(B) Heat map plots of PolII recruitment at Ensembl mouse genes (±2 Kb) from resting and activated B cells.

(C) Density graph showing PolII occupancy near TSSs in G_0 (blue line) and cycling B cells (red line). The upper value of the composite data set is shown with a dotted line. The resting maximal PolII average density is 16 bp from TSS, the activated maximal is 34 bp.

See also Figure S1.

2012). To directly address these possibilities, we measured the absolute number of mRNA transcripts in G_0 and cycling B cells by spiking-in 96 mRNA standards to total RNA isolated from 10^6 cells prior to transcriptome (mRNA-seq) analysis. This normalization revealed that mRNA copy numbers of the vast majority of ORFs increased, on average, 11.7-fold during activation (Spearman's test, $\rho = 0.78$; Figure 1C and Figure S1A available online). Thus, rather than upregulating a specific subset of transcripts, B cell activation amplifies the entire gene expression program of G_0 cells.

To determine whether transcriptome amplification correlated with epigenetic changes, we quantified histone acetylation in resting and activated B cell populations using reverse-phase protein microarray (RPMA) (Calvo et al., 2008). In this assay, the absolute concentration of histone modifications per million cells is calculated directly from lysates printed in microarrays. As such, protein measurements are not influenced by epitope masking or potential differences in chromatin condensation between cell types (Calvo et al., 2008). We found that LPS+IL4 activation induced a 3- to 7-fold increase in the total levels of acetylation (Ac) for histones H3K14, H3K23, H4K5, H4K8, and H4K16 ($p < 0.003$; Figure 1D). Notably, there were little or no changes in overall H2AK5Ac, H3K9Ac, or H3K18Ac under the same conditions (Figure 1D). Thus, although, as a group, acetylation marks are activating in nature (Wang et al., 2008; Yamane et al., 2011), lymphocyte differentiation increments global acetylation of some but not all histone lysines. Importantly, and in line with transcriptome amplification, H3K14Ac, H3K23Ac, H4K5Ac, H4K8Ac, and H4K16Ac increased proportionally during stimulation, as determined by ChIP-seq analysis (Spearman's test, $\rho = 0.69$; Figure 1E). Altogether, the findings show that cycling lymphocytes undergo a proportional amplification of mRNA synthesis and acetylation of specific histone lysines.

Also consistent with transcriptome amplification, the number of genes recruiting PolII was essentially unaffected during activation (Figure 2A). This result implies that few genes are transcribed de novo upon B cell differentiation. Exceptions were 461 and 1,168 genes that were preferentially expressed in resting or activated B cells (Figure 2A). Notably, although mRNA copy numbers increased on average more than 10-fold in cycling lymphocytes (Figure 1C), ChIP-seq analysis revealed only a modest increase (1.7-fold) in PolII promoter occupancy relative to G_0 (Figure 2B). Thus, the extent of transcriptome amplification during B cell activation cannot be explained on the basis of PolII promoter recruitment.

To explore whether transcriptome amplification correlates with changes in promoter-proximal pausing, we analyzed PolII composite profiles. In activated B cells, maximal polymerase density occurred ~35 bp downstream of TSSs (Figure 2C), a result that is in agreement with the location of PolII pausing in mouse embryonic stem cells (Rahl et al., 2010). Notably, PolII in resting B cells displayed an average upstream shift of nearly 20 nucleotides in comparison to cycling counterparts (Figure 2C). This result indicates that the transition from abortive to productive elongation is kinetically limiting in G_0, causing RNA polymerases to be localized nearer to TSSs. Thus, basal transcription in naive lymphocytes correlates with a delay in PolII prepause progression.

A Genome-wide Map of ssDNA

PolII promoter escape from TSSs to the pausing site is preceded by open complex formation (Margaritis and Holstege, 2008). Thus, we entertained the possibility that limited transcription in G_0 lymphocytes might reflect inefficient promoter melting. To test this idea globally, we combined chemical and enzymatic techniques to map ssDNA across the mammalian genome by high-throughput sequencing (ssDNA-seq). The approach makes use of $KMnO_4$ treatment, which modifies ssDNA in living cells by oxidizing pyrimidine bases with a marked preference for exposed thymidine residues (Mirkovitch and Darnell, 1992). Because oxidized bases are unable to base pair with the complementary strand, they become susceptible to mung bean nuclease cleavage (Figure 3A). The resulting double-stranded DNA ends are then 3′-tailed with terminal deoxynucleotidyl transferase (TdT) in the presence of biotinylated nucleotides. Finally, samples were sonicated to ~200 bp, and biotinylated DNA was streptavidin selected prior to Illumina library preparation (Figure 3A). To avoid the biotinylation of preexisting DNA breaks, we blocked samples prior to nuclease treatment by incubation with chain-terminating cordycepin-5′-triphosphate and

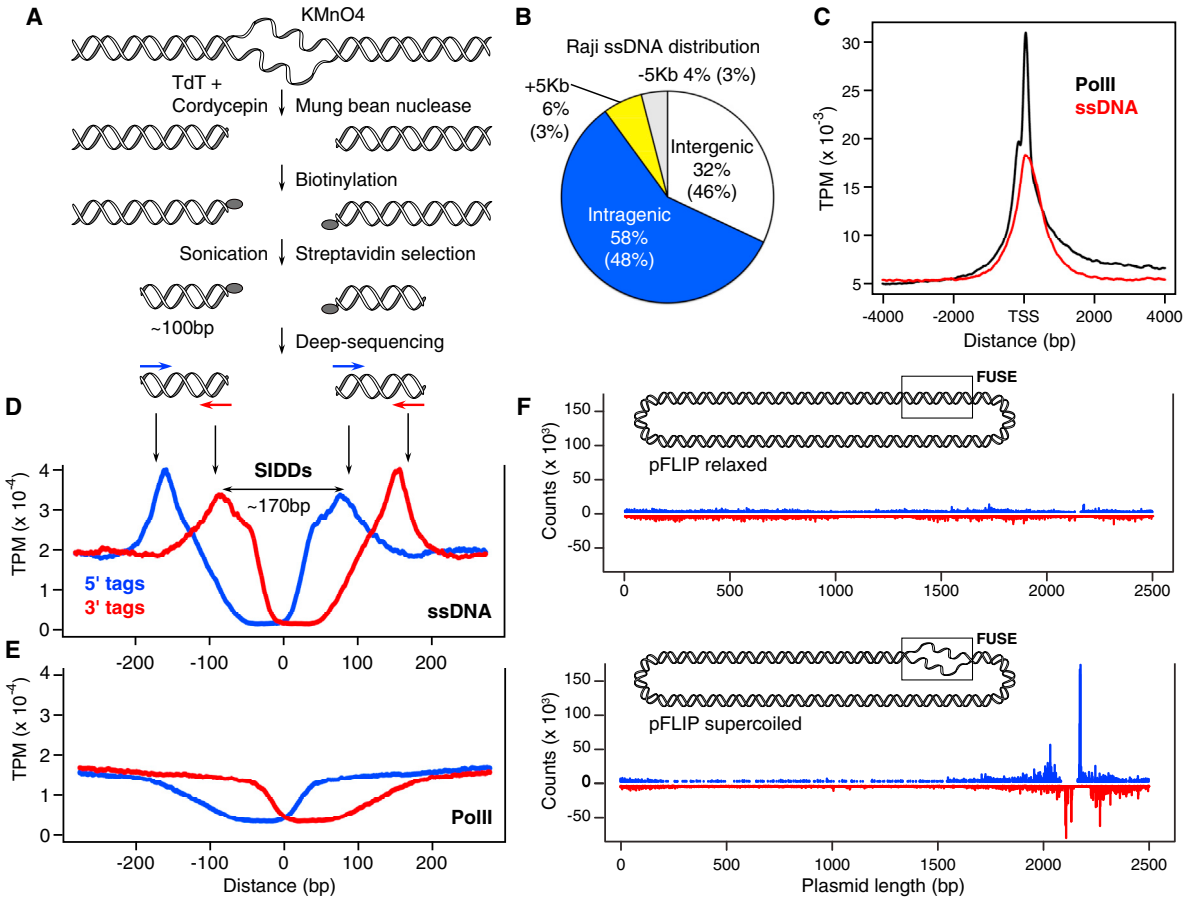

Figure 3. ssDNA-Seq Approach and Validation

(A) During ssDNA-seq, ssDNA is stabilized in live cells by treatment with $KMnO_4$, which selectively oxidizes exposed thymidines. Cordycepin and TdT are used to block pre-existing 3′ DNA free ends, and ssDNA is digested with mung bean nuclease. Then, DNA ends exposed by nuclease treatment are biotinylated and, following sonication, streptavidin selected and deep sequenced.

(B) Distribution of ssDNA signals in Raji cells. +5 Kb and −5 Kb represent ssDNA signals aligning within 5 Kb upstream of TSS or downstream of gene stop codons, respectively. Numbers in parenthesis are the expected percentages for randomly distributed reads.

(C) Composite diagram showing ssDNA and PolII signals around TSSs of human genes in Raji cells.

(D) Composite diagrams showing the distribution of 5′ (blue) and 3′ (red) ssDNA-seq tags around SIDDs predicted for the mouse genome.

(E) Deep-sequencing profiles at mouse SIDDs obtained with antibodies against PolII.

(F) ssDNA-seq analyses of relaxed (upper) or supercoiled (lower) pFLIP plasmids containing human *Myc* FUSE element. ssDNA-seq 5′ and 3′ tags are represented in blue and red, respectively.

See also Table S1.

TdT (Figure 3A and Experimental Procedures). The specificity of the ssDNA-seq protocol for melted DNA was evident from the observation that $KMnO_4$-untreated samples yielded consistently ~20-fold less DNA than treated ones (Table S1A).

First, we applied ssDNA-seq to the human Burkitt's lymphoma line Raji and LPS+IL4-activated mouse B cells. Deep-sequencing generated a total of 125 million sequence reads from three independent Raji experiments (Table S1B). At this range, specific signal reached near saturation (Figure S1B). Biological replicates confirmed that ssDNA-seq was highly reproducible (Spearman's test, $\rho > 0.9$; Figure S2A). We found ssDNA island distribution to be biased for genic domains in Raji. Nearly 60% of ssDNA signals were directly associated with genes, an additional 10% aligning within 5 kb upstream of TSSs or downstream of stop codons (Figure 3B). The remaining 32% were aligned to intergenic domains (Figure 3B). This enrichment was higher than expected when tags were uniformly distributed (Figure 3B, values in parentheses). Within genes, a composite analysis revealed an ssDNA peak that was maximal at TSSs and extended approximately 1.5 kb on either side (Figure 3C). This peak, which represented 12% of ssDNA signals within genes, overlapped precisely with the profile of PolII occupancy (Figure 3C).

In addition to sites of gene expression, ssDNA is expected to be associated with simple DNA repeats or AT-rich domains, which adopt thermodynamically unstable DNA conformations or non-B DNA in the presence of negative supercoiling (Kouzine et al., 2008). In spite of extensive in vitro characterization, little is

known about the topology, stability, and distribution of non-B DNA in living cells. To further validate the ssDNA-seq assay, we scanned activated B cell libraries for sequence tags associated with sites of stress-induced DNA duplex destabilization (SIDD), as predicted in silico (Benham and Bi, 2004). Using a destabilization energy $G(x) \leq 3$ kcal/mol, the algorithm identified a total of 1,057,816 SIDDs in the mouse genome. Similar results were obtained in Raji cells (data not shown). A composite analysis of these sites revealed a remarkably well-defined ssDNA-seq profile, two pairs of peaks surrounding the predicted SIDDs (Figure 3D). Each peak pair, composed of 5′ (+ strand) and 3′ (− strand) sequence tags, mirrored the 200 bp average size of ssDNA-seq libraries (Figures 3A and 3D and Experimental Procedures).

The extent of DNA melting at SIDDs, defined as the average distance separating the innermost boundaries of the peak pairs, was ~170 bp (Figure 3D). SIDD melting was not the direct result of PolII activity, given that we could not detect PolII occupancy at these sites (Figure 3E). Interestingly, both the ssDNA and PolII IPs displayed a distinct depression in signal within SIDD sites. Comparable results were obtained upon immunoprecipitation of CTCF, which, like PolII, is not directly recruited to SIDDs (Figure S2B). This profile can be explained by non-B DNA susceptibility to sonication and T4 exonuclease activity during deep-sequencing library preparation (Figure S2C). We conclude that, in addition to promoter melting, the ssDNA-seq protocol reveals both the location and topological features of non-B DNA in mammalian cells.

As an independent confirmation of the ssDNA-seq protocol, relaxed and supercoiled plasmids were treated with $KMnO_4$, and DNA melting was measured by ssDNA-seq. The plasmids carried *Myc* far upstream element (FUSE) (Kouzine et al., 2008), a SIDD site that readily melts as supercoilicity at the *Myc* promoter builds up during transcription (Kouzine et al., 2004). The superhelical density of the topoisomers (n = 4) was monitored with agarose gels (see Experimental Procedures). Deep-sequencing only showed extensive melting of FUSE in the presence of torsional stress (Figure 3F). Importantly, the melting profile of FUSE closely recapitulated that obtained from SIDD sites in vivo, and two pairs of strand-specific peaks surrounded the melted domain (Figures 3F and 3D). Thus, the ssDNA-seq protocol can detect bona fide ssDNA with high specificity.

Melting of Promoters and Active Enhancers in Primary B Cells

Similar to Raji, ssDNA in mouse B cells was biased for genic (±5 Kb) rather than intergenic domains (59% versus 41%, respectively; Figure 4A). Likewise, we found an overall correlation between ssDNA, PolII recruitment, and gene expression in primary B cells. For instance, Figure 4B shows extensive ssDNA across the highly transcribed *H2afx* gene, whereas the signal was less pronounced at flanking *Hmbs* and *Dpagt1* genes, which exhibit comparatively less PolII occupancy and mRNA synthesis. To validate these observations across all genes, we analyzed ssDNA as a function of global gene expression. On the basis of the bimodal distribution of the activated B cell transcriptome (Figure 4C), we classified mouse genes into three main transcription groups: high (12,993), low (8,829), and silent (9,186). The analysis showed the extent of ssDNA correlated with the levels of transcription in each of the groups (Figure 4D). Considering that ssDNA-seq specifically oxidizes thymidine residues, it is important to point out that the results were not influenced by promoter CpG (or AT) contents, which, in B lymphocytes, are highest in lowly expressed genes (Figure S3A). Thus, ssDNA-seq accurately recapitulates the location and extent of DNA melting associated with gene expression.

On the basis of PolII binding profiles (Rahl et al., 2010), we further classified transcribed genes into paused (pausing index $[P_i] > 10$) and elongating ($1 \leq P_i \leq 10$). P_i is a measure of the ratio of PolII density at promoter versus gene body and directly reflects the dynamics of PolII assembly and pause release (Rahl et al., 2010). In paused genes, the rate of promoter clearance is relatively lower than that of assembly, resulting in PolII accumulation at promoter-proximal sequences (Muse et al., 2007; Zeitlinger et al., 2007). Conversely, elongating genes exhibit a higher rate of pause release, and, thus, PolII can be readily immunoprecipitated along gene bodies (Figure S2D) (Muse et al., 2007; Zeitlinger et al., 2007). Consistent with these dynamics, there was substantial ssDNA at promoter-proximal sequences (~1 kb around TSSs) of paused genes (Figure 4E), whereas elongating genes displayed less DNA melting at promoter domains concomitant with higher melting at gene bodies (Figure 4E). Thus, these findings are consistent with the notion that DNA melting around TSSs is inversely proportional to the rate of PolII pause release.

In addition to promoters, PolII is recruited to a subset of active intergenic $p300^+$ enhancers, where it has been shown to synthesize small enhancer RNAs (eRNAs) (Kim et al., 2010). To determine whether enhancer transcription is associated with DNA melting, we compared ssDNA islands with p300 genomic occupancy in activated B cells (Kuchen et al., 2010). $p300^+$ enhancers were distinguished from promoters by virtue of being located distally from annotated TSSs while being associated with high H3K4me1 (Heintzman et al., 2007; Kim et al., 2010) and low H2AZ deposition (Figures 4F and S3B). Conversely, promoters were mostly $p300^+H3K4me1^{low}H2AZ^{high}$ (Figure 4F). We found PolII present at 81% of $p300^+$ intergenic enhancer islands (3,234 of 3,994 sites) and 98% of $p300^+$ promoter islands (4,339 of 4,392 sites; Figure 4G). By contrast, we found evidence of DNA melting in just 13% of $p300^+$ enhancers, whereas more than 86% of $p300^+$ promoters were associated with ssDNA (Figure 4G). This difference in DNA melting is consistent with transcriptional activity being more pronounced at promoters relative to enhancers (Kim et al., 2010). Similar to TSSs, the composite profile of ssDNA at enhancers overlapped with the peak of PolII recruitment (Figure 4H), and eRNA synthesis (Figure S4). Altogether, our observations demonstrate that ssDNA-seq reliably detects DNA melting at enhancers in a manner proportional to the extent of PolII recruitment and activity.

Limited Promoter Melting and TFIIH Expression in G_0 Lymphocytes

Having validated the ssDNA-seq approach, we next analyzed promoter melting in resting splenic B cells. A total of 41 million sequence tags were obtained from two independent ssDNA-seq experiments (Table S1B). The inter- and intra-genic

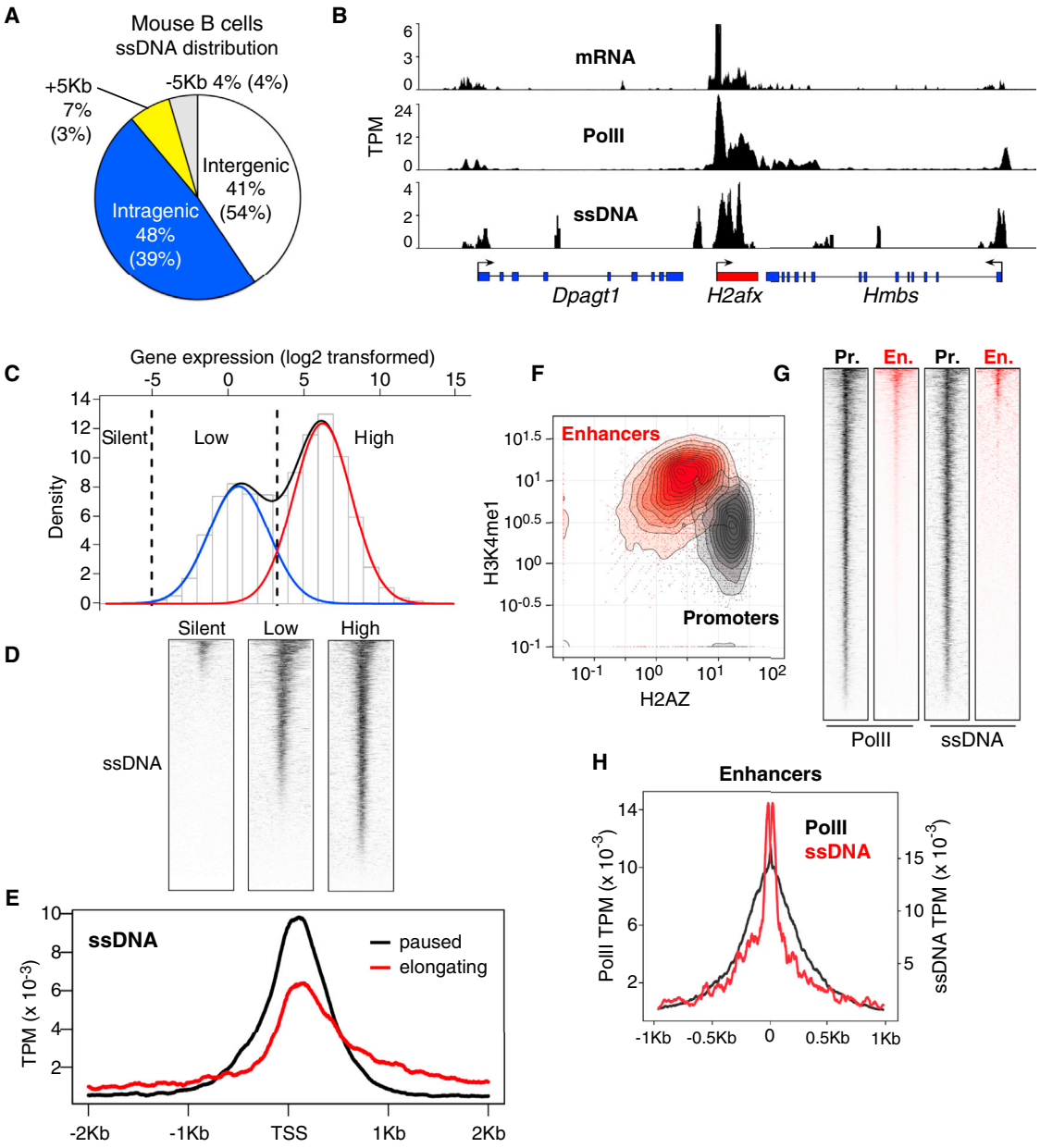

Figure 4. ssDNA-Seq Profiles in Primary B Cells

(A) Distribution of ssDNA signals in primary LPS+IL4 activated B cells.

(B) Correlation between mRNA transcripts, PolII recruitment, and ssDNA at *Dpagt1*, *H2afx*, and *Hmbs* genes. Data are represented as sequence tags per million (TPM).

(C) Bimodal distribution of gene expression in activated B cells. Red and blue lines delineate first and second components, respectively. Black dashed lines demarcate the threshold for highly expressed, lowly expressed, and silent genes.

(D) Heat map of ssDNA-seq profiles around TSSs (±2 Kb) for high, low, and silent gene groups defined in (C).

(E) ssDNA composite alignment at elongating ($1 \leq Pi \leq 3$, red line) and paused ($Pi \geq 10$, black line) genes.

(F) Density graph, p300^{+} islands associated with enhancers (H3K4me1^{high}H2AZ^{low}) or promoters (H3K4me1^{low}H2AZ^{high}). Data were normalized as fold enrichment.

(G) Heat maps showing PolII and ssDNA at p300^{+} promoter (gray) or enhancers (red).

(H) Alignment of PolII (black line, left y axis) and ssDNA (red line, right y axis) at p300^{+}H3K4me1^{high}H2AZ^{low} enhancers.

See also Figures S2–S4.

distribution of ssDNA signals was similar between resting and activated B cells (compare Figure S5A to Figure 4A). However, visual inspection of the aligned data revealed a substantial reduction in PolII-associated DNA melting across the genome of naive cells. For instance, Figures 5A and S5B show extensive ssDNA at promoters of *Sfi1* and *Smg9* genes in cycling cells,

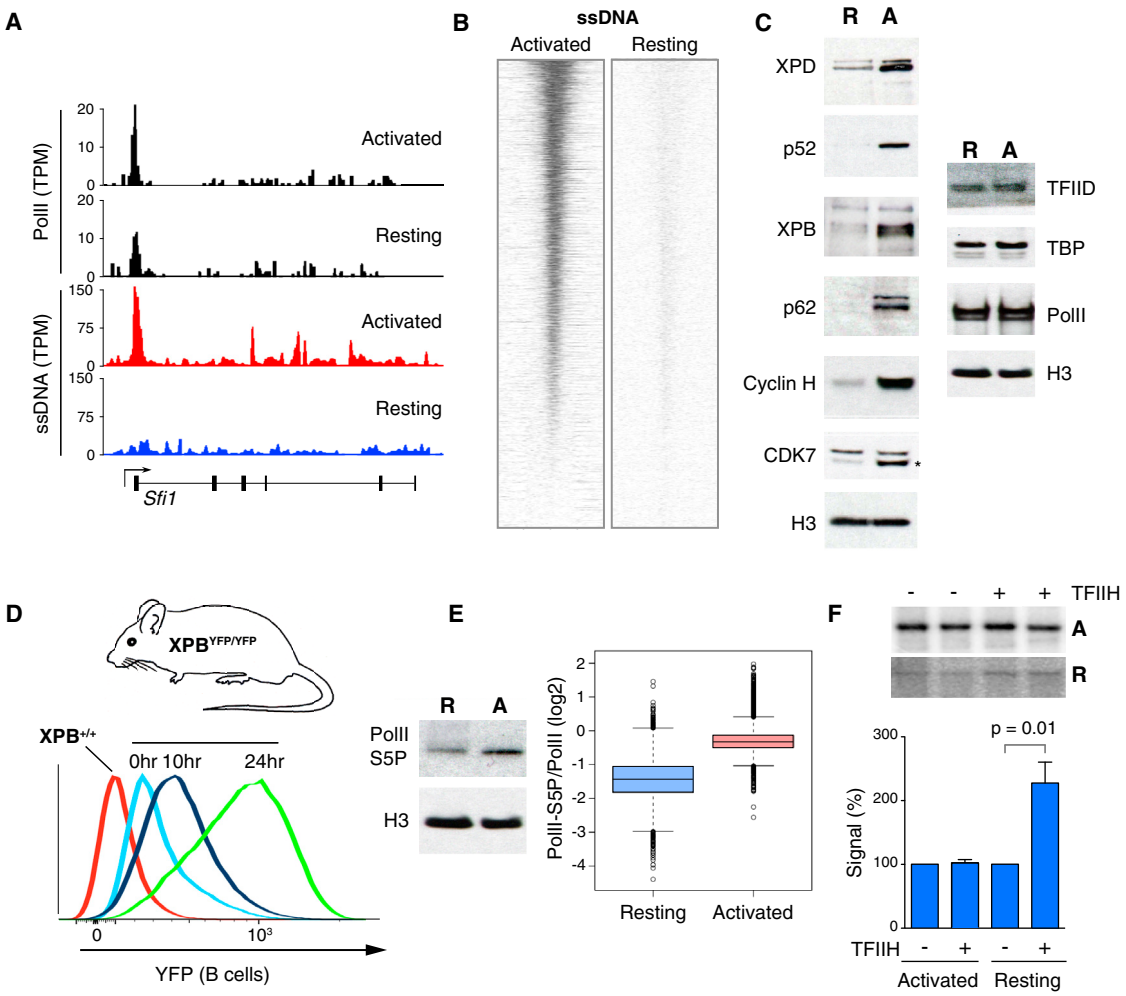

Figure 5. Reduced Promoter Melting and TFIIH Levels in G_0

(A) PolII and ssDNA density determined at *Sfi1* gene in resting and activated B cells. Data were normalized as sequence tags per million (TPM).

(B) Heat map plots of ssDNA at Ensembl mouse genes (± 2 Kb) from activated and resting B cells.

(C) Left, TFIIH subunit protein levels measured in resting (R) and 48 hr LPS+IL4-activated (A) B cells by western blot. Right, PolII subunits and the general transcription machinery.

(D) XPB helicase protein levels measured in $XPB^{YFP/YFP}$ B cells or $XPB^{+/+}$ controls. Lymphocytes were activated with LPS+IL4 for 24 hr, and YFP expression was monitored by flow cytometry.

(E) Left, western blot measurement of PolIIS5P during activation. Gel loading was normalized per total protein content. Right, box plots represent the ratio of PolII-S5P versus total PolII in resting (blue) and activated (red) B cells as determined by ChIP-seq analysis. Values were normalized as TPM per total PolII-S5P and PolII per cell.

(F) In vitro transcription of a linear DNA template (pG5HM [C_2AT] plasmid) carrying a minimal promoter. DNA was incubated with equal amounts (80 ng) of nuclear cell extracts. Reactions were complemented (+) with affinity-purified TFIIH. The bar graph compares transcription levels between TFIIH-complemented reactions (+) and those without TFIIH (−). Transcription in noncomplemented reactions was set up to 100%. Data represent the mean values ± SEM; n = 6 for all samples. See also Figures S5 and S6.

respectively, whereas we detected little or no ssDNA in the same genes in naive counterparts. Conversely, PolII recruitment at promoters from both genes was comparable between the two cell types (Figures 5A and S5B). To extrapolate these observations to the entire genome, we generated heat maps of ssDNA gene profiles from resting and activated B cells. In stark contrast to PolII recruitment, which was comparable between the two cell types (Figure 2B), most promoters showed little or no melting in G_0 (Figure 5B). The results demonstrate that open complex formation is limited across the genome of naive cells. In contrast, ssDNA associated with PolI ribosomal DNA (rDNA) transcription, which does not directly depend on transcription factor IIH (TFIIH) activity for promoter melting (Assfalg et al., 2012), was readily detected in the same cells (Figure S5C). Furthermore, low levels of ssDNA in G_0 cells were not due to cell-cycle arrest per se, given that serum-starved human fibroblasts displayed similar levels of promoter melting in comparison to cycling counterparts (Figure S5D). In conclusion, the data argue that PolII

complexes in naive lymphocytes are found in a relatively closed configuration, whereas cell activation promotes global open complex formation and extensive gene expression.

The formation of a stable transcription bubble requires TFIIH, an 11-subunit complex that includes XPB and XPD helicases directly involved in DNA melting (Guzmán and Lis, 1999; Holstege et al., 1996). Notably, the expression of TFIIH subunits was substantially decreased in G_0 B cells, as determined by western blot (Figure 5C). This included members of the TFIIH core (p52, p62, XPB, and XPD) and the CAK complex (cyclin H and CDK7). A comparison of naive and CD3-, CD28-, and IL-2-activated mouse T cells showed similar results (Figure S6A), indicating that TFIIH is also limiting in G_0 T lymphocytes. In contrast, we found little or no differences in the expression of the basal transcription factor A (TFIIA), TATA-binding protein (TBP), or total PolII during B cell activation (Figure 5C). Within the context of differentiation, TFIIH subunits were reproducibly low or undetected in resting cells (Figure S6B), even though their transcripts were moderately to highly expressed (Figure S6C). However, as early as 30 hr postactivation, we observed a marked increase in p62, cyclin H, p52, and XPD transcripts and protein levels (Figures S6Dand S6B, respectively). At ~10 hr postactivation, TFIIH levels were comparable to those observed in bone marrow pro- and pre-B cells (Figure S6B). Similar dynamics were observed by activating B lymphocytes carrying TFIIH XPB helicase fused to the yellow fluorescent protein ($XPB^{YFP/YFP}$ mice, (Giglia-Mari et al., 2009) (Figure 5D). On the basis of these results, we conclude that the steady-state levels of the promoter-melting complex TFIIH are substantially reduced as B cells exit the bone marrow and rapidly restored upon activation.

In addition to promoter melting, TFIIH plays additional roles in transcription initiation, including the phosphorylation of PolII C-terminal heptad repeats at serine 5 (PolII-S5P) (Feaver et al., 1994; Liao et al., 1995; Sterner et al., 1995), a feature that, in turn, facilitates the extension of the transcription bubble from the TSS to the promoter-proximal pausing site (Dvir, 2002). Consistent with limited TFIIH expression, PolII-S5P levels in naive B cells were ~5× lower than in dividing counterparts, as determined both by western blot and deep-sequencing (Wilcoxon test, $p < 1.0 \times 10^{-100}$; Figure 5E). This difference was readily apparent at genes programmed for abundant transcription after cellular activation (Figure S5E).

The reduction in promoter melting (Figure 5B), the low levels of PolII-S5P (Figure 5E), and the observed delay in open complex extension (Figure 2C) supports the view that TFIIH activity is limiting in G_0. Then, we explored whether gene expression in resting cells can be complemented by the addition of TFIIH. To this end, we prepared nuclear cell extracts from resting and activated B cells and performed in vitro transcription of a linear DNA template containing a minimal core promoter (Ohkuma et al., 1995). Western blot analysis of the extracts confirmed little or no differences in total PolII or TBP but confirmed a substantial decrease in TFIIH p62 in G_0 (data not shown). Consistent with basal transcriptional activity in G_0, we observed a ~20-fold difference in in vitro transcription levels between naive and 72 hr activated B cell extracts (Figure 5E). The addition of affinity-purified TFIIH did not alter the transcription output of activated B cell extracts (Figure 5F). When added to G_0 extracts, TFIIH consistently increased basal transcription by ~2-fold ($p = 0.01$; Figure 5E); however, this increase was modest and never reached the levels obtained with activated B cell extracts (Figure 5E). Thus, additional activities beyond TFIIH expression are required to fully complement the G_0 transcription machinery in this assay.

TTD Cells Show Defects in Promoter Melting

Similar to naive lymphocytes, TFIIH expression levels are reduced in trichothiodystrophy (TTD) patient fibroblasts. The TTD syndrome is caused by mutations in TFIIH subunits, including XPB and XPD helicases, and results in ultraviolet sensitivity, mild mental retardation, ichthyosis, and recurrent infections (Vermeulen et al., 1994). Although the TTD phenotype is, in part, ascribed to XPD's role in nucleotide excision repair, crippled transcription is also believed to contribute to the severity of the disease (de Boer et al., 1998; Vermeulen et al., 1994). In this context, some TTD patients carry XPD temperature-sensitive mutants and display fever-dependent transcriptional defects (Vermeulen et al., 2001). In particular, fibroblasts isolated from such patients grow normally at 37°C but, at higher temperatures, express low levels of TFIIH and an overall reduction in transcription (Vermeulen et al., 2001). To strengthen the link between TFIIH expression and the extent of promoter melting in vivo, we analyzed TTD fibroblasts by ssDNA-seq. Relative to 37°C, western blot confirmed the reduced expression of XPD as well as Cdk7 in TTD fibroblasts grown at 41°C, but not in cells reconstituted with wild-type XPD (Figure 6A). Also consistent with previous findings, TTD fibroblasts displayed reduced mRNA synthesis and defects in cell proliferation at 41°C (Figure 6B) (data not shown). As determined by ssDNA-seq, these features were correlated with an overall reduction in promoter melting in comparison to control or TTD cells grown at 37°C (Figure 6C). Thus, the data demonstrate that promoter melting across the genome is tightly linked to TFIIH expression levels. Furthermore, the findings provide a mechanistic rationale for reduced mRNA synthesis and, potentially, the immunodeficiency observed in trichothiodystrophy syndrome patients.

DISCUSSION

Seminal work in the 1960s and 1970s revealed that lymphocytes undergo a rapid transformation when exposed to mitogens, including a dramatic increase in cell size, histone acetylation, RNA synthesis, and protein production (Jaehning et al., 1975; Keller, 1975; Pogo et al., 1966, 1967). In vivo studies have since corroborated these initial observations by showing that both primary and memory responses activate G_0 B and T cells in a matter of hours (Shapiro-Shelef and Calame, 2005). However, although the extracellular and intracellular signals involved have been characterized extensively, the nuclear mechanisms driving rapid activation of lymphocytes are unknown. Our findings shed new light on this issue by showing that the transcriptomes of naive and stimulated lymphocytes are remarkably alike in that, whereas transcription increases ~10-fold upon activation, the number of genes and their relative expression in the two stages are largely proportional. The strong inference is that the

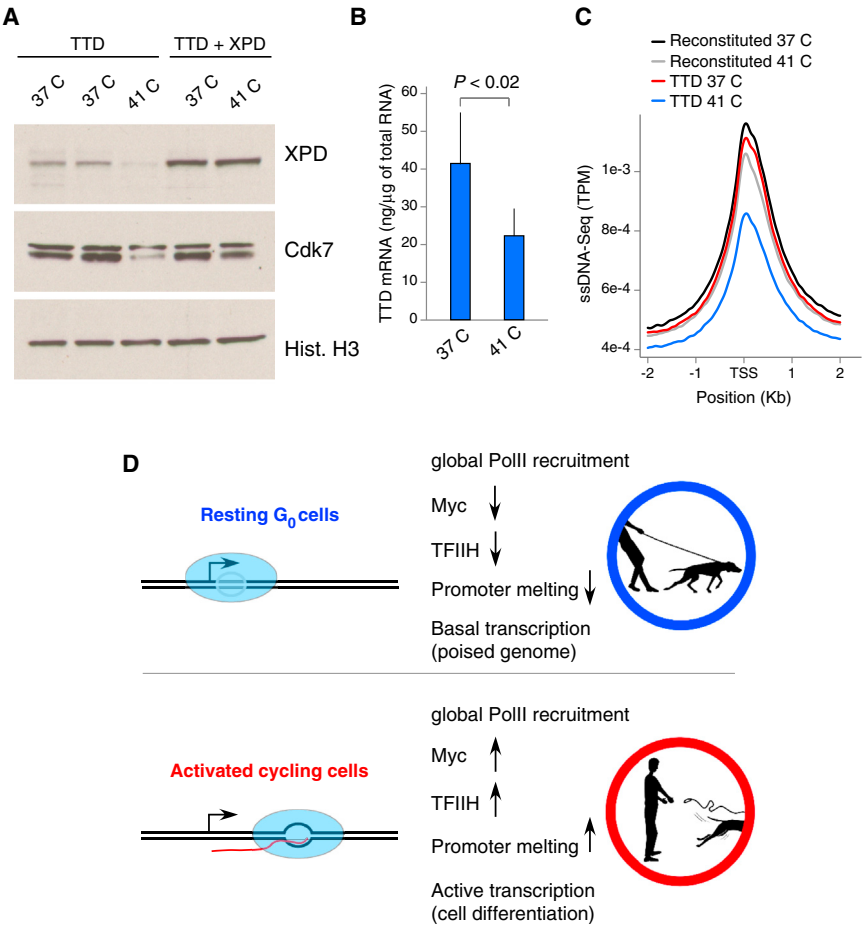

Figure 6. TFIIH Expression Correlates with the Extent of Transcription and Promoter Melting in XPD Patient Fibroblasts

(A) XPD and Cdk7 protein levels in fibroblasts isolated from TTD patients carrying an XPD temperature-sensitive mutant. TTD + XPD denotes fibroblasts reconstituted with wild-type XPD. Cells were grown at 37°C or 41°C for at least 72 hr.

(B) mRNA levels in TTD fibroblasts grown at 37°C or 41°C. Data represent the mean values ± SEM; n = 4 for all samples.

(C) Composite profiles of ssDNA in TTD or reconstituted fibroblasts grown at the two temperatures.

(D) The findings indicate that resting lymphocytes hold tightly their transcriptome "on a leash" by allowing the mostly normal recruitment and assembly of PolII while limiting promoter melting. This scenario might be the result of low levels of TFIIH, Myc, and/or potentially additional mechanisms (upper schematics). Upon activation, extensive melting and a rapid shift from basal to full transcriptome expression correlates with stabilization of TFIIH and Myc protein levels (lower schematics).

transcriptome of naive cells is poised, or in latent form, for rapid cellular induction.

Our studies argue that transcriptome poising in G_0 cells is achieved, at least in part, by allowing a mostly normal assembly of PolII at promoters while globally restricting open complex formation. In *E. coli*, the transition from closed (RP_c) to open (RP_o) complex formation is facilitated by the combined action of transcriptional activators and *cis*-regulatory elements (Liu et al., 2004; Lutz et al., 2001). It has been proposed for some time that eukaryotes might also regulate the dynamics of transcription by controlling promoter melting. However, this has been difficult to ascertain because of the challenge of quantitatively monitoring melted DNA in a large number of promoters simultaneously. Several laboratories, including ours, have recently used RPA-seq (Hakim et al., 2012; Yamane et al., 2011; Yamane et al., 2013), Rad51-seq (Di Virgilio et al., 2013; Khil et al., 2012; Yamane et al., 2013), and Rad52-seq (Zhou et al., 2013) to map ssDNA in mammalian cells. However, these approaches cannot detect promoter melting and only identify sites undergoing DNA end resection during repair by homologous recombination. The ssDNA-seq protocol now provides a means to visualize and quantify nonduplex DNA in living cells. With this technique, we were able to establish that open complex formation in eukaryotic cells can be globally regulated in response to cell-cycle and environmental cues. This is in addition to holoenzyme recruitment and promoter-proximal pausing, which, to date, are the only other known rate-limiting steps of gene expression in higher organisms (Margaritis and Holstege, 2008).

Precisely how G_0 lymphocytes inhibit open complex formation is unclear. One possibility for how they inhibit this formation is by controlling TFIIH protein levels, which we found to be tightly linked to the extent of promoter melting during B cell ontogeny. The role of TFIIH in promoter melting has been well established by KMnO4 footprinting analysis of several promoters (Holstege et al., 1997; Holstege et al., 1996; Kim et al., 2000), the characterization of early steps of gene expression (Guzmán and Lis, 1999), and the ability of TFIIH to melt relaxed plasmids ex vivo (Goodrich and Tjian, 1994; Parvin and Sharp, 1993). Furthermore, we have shown that promoter melting is proportional to TFIIH expression and activity in TTD patient fibroblasts. At the same time, our in vitro transcription studies imply that the role of TFIIH in the process of transcriptome amplification is most likely complemented by additional activities. Particularly, we have recently shown that the transcription factor Myc acts as a universal amplifier of transcription in B cells by associating with preactive genes and increases overall expression (Nie et al., 2012). Similar to TFIIH, Myc protein levels peak as lymphocytes enter the cell cycle (Nie et al., 2012). Here, we have shown that activating histone acetylation represents yet another process that is proportionally enhanced in lymphocytes in response to mitogenic signals. Thus, transcriptome amplification might result from the coordinated activity of TFIIH, general transcription factors including Myc, and epigenetic marks. We propose that, within the cadre of the immune response, these processes allow quiescent lymphocytes to hold the

transcriptome "on a leash" or a poised state that can be promptly reverted in the presence of pathogens (Figure 6D). Considering that the TFIIH CDK7 subunit also controls cell-cycle entry by virtue of its ability to phosphorylate and activate cyclin-dependent kinases (Dvir, 2002; Klemsz et al., 1989), the model also helps explain the link between transcriptome amplification and cell-cycle initiation.

In addition to the dynamics of promoter melting, the ssDNA-seq protocol provides a unique view of the location and conformation of non-B DNA. Recent computer-based thermodynamic searches have uncovered a large number of sequences across the mammalian genome that can potentially form non-B DNA in vivo (Cer et al., 2011). Intriguingly, these sequences localize preferentially to defined genomic sites, and mounting evidence indicates that they may play an important physiological role. Analyses of human cells, for instance, have uncovered a correlation between predicted G4 quadruplexes at promoters and the extent of gene expression (Du et al., 2008). Furthermore, at skeletal muscle promoters, formation of G4 quadruplexes impacts the recruitment of MyoD during differentiation (Shklover et al., 2010; Yafe et al., 2008). Similarly, transcription-induced DNA supercoiling controls the firing rate of the *Myc* promoter (Kouzine and Levens, 2007). From a translational point of view, DNA topology is also noteworthy because human fragile sites implicated in genomic instability and tumorigenesis often map to predicted non-B DNA structures (Barlow et al., 2013; Raghavan and Lieber, 2006). We anticipate that ssDNA-seq will be instrumental to comprehensively study the location and dynamics of non-B DNA under physiological conditions.

EXPERIMENTAL PROCEDURES

Resting naive mouse B cells were isolated from splenocytes with anti-CD43 MicroBeads (Miltenyi Biotec) by negative selection and activated for 72 hr in the presence of LPS (50 $\mu g/ml^{-1}$ final concentration, *E. Coli* 0111:B4; Sigma-Aldrich) + IL4. (2.5 ng/ml final concentration, Sigma-Aldrich). Apoptotic cells were removed with a Dead Cell Removal Kit (Miltenyi) followed by Ficoll gradient with >90% live-cell purity. To minimize the influence of DNA replication on the pattern of ssDNA across genome, we arrested Burkitt's lymphoma Raji cells in G1 by treatment with 1.5% (v/v) DMSO for 96 hr as previously described (Sawai et al., 1990). To remove DMSO, we pelleted cells at 600 × *g* for 5 min and resuspended them in fresh medium at 10^6 cells/ml. Samples were processed 6 hr later when cells were synchronized at the G1 phase of the cell cycle. For ssDNA-seq, cells were processed as described in the following sections.

Potassium Permanganate Treatment

First, 8 × 10^7 cells were washed with PBS at 37°C and resuspended in 15 mM TRis-HCl (pH 7.5), 60 mM KCl, 15 mM NaCl, 5 mM $MgCl_2$, and 300 mM sucrose. Then, cells were treated with 40 mM $KMnO_4$ for 70 s at 37°C. The reaction was quenched by the addition of EDTA, β-mercaptoethanol, SDS, and RNase-DNase-free to final concentrations of 50 mM, 700 mM, 1% (w/v), and 40 μg/ml, respectively, followed by 1 hr incubation at 37°C. Proteins were digested by the addition of proteinase K to a final concentration of 300 μg/ml and incubated overnight at 37°C. DNA was extracted twice with phenol, once with phenol:chloroform, and precipitated in the presence of 2 M ammonium acetate with two volumes of ethanol. The pellet was washed in 75% ethanol and resuspended in 1 ml of Tris and EDTA (TE) buffer. In parallel control experiments, instead of $KMnO_4$ solution, cells were incubated with an equal volume of water, and DNA purification was performed as described above.

Blocking of Unspecific DNA Breaks

To block any free 3′ DNA ends formed either by topoisomerase activity in vivo or mechanical shearing during sample preparation, cordycepin-5′-triphosphate was incorporated on DNA with TdT as previously described (Tu and Cohen, 1980). Because cordycepin-5′-monophosphate lacks a 3′-OH group, only a single nonextendable residue is incorporated per DNA strand. DNA samples were incubated with 800 U of TdT (New England Biolabs), 1× TdT buffer, and 120 μM of cordycepin-5′-triphosphate sodium salt (Sigma-Aldrich) in a final volume of 3 ml at 37°C for 1 hr, followed by a single phenol:chloroform extraction and precipitation in the presence of 2 M ammonium acetate with two volumes of ethanol. The DNA pellet was resuspended in 1 ml of TE buffer.

Generation of Biotinylated DNA Breaks

DNA samples were divided into four microtubes (250 μl each) and treated with 0, 100, 200, or 300 U of mung bean nuclease (NE Biolabs) in a 600 μl final volume. Samples were incubated for 30 min at 30°C, and DNA was purified as described above and dissolved in 100 μl of TE buffer. DNA size was determined by gel electrophoresis, and its concentration was measured with a NanoDrop (ND-1000, Thermo Scientific) spectrophotometer. Then, 50 μg of DNA from each microtube was biotinylated by 3′-end tailing reaction in 400 μl of 1× TdT buffer (Roche) with 4,000 U TdT (Roche), 0.5 mM dCTP, and 0.08 mM Biotin-16-dUTP (Roche) at 37°C for 15 min. Reactions were stopped by adding EDTA to a 20 mM final concentration. To remove unincorporated biotin, samples were extracted with phenol:chloroform, precipitated twice with 2 M ammonium acetate and two volumes of ethanol and dissolved in 200 μl of TE buffer.

Capture of Nuclease-Digested DNA Ends

Nuclease-digested biotinylated DNAs were sonicated in order to generate 150–450 bp DNA fragments. Sonication was performed with an ultrasonic sonicator (Bioruptor [Diagenode] at high power) by pulsing 20 times for 20 s and incubating on ice for 30 s between each pulse. Then, biotinylated fragments were captured with streptavidin-coated beads (Dynabeads kilobaseBINDER Kit, Dynal) according to the manufacturer's protocol. After extensive washing with 10 mM Tris-HCl (pH 7.5), 1 mM EDTA, and 2.0 M NaCl, biotin-streptavidin complexes were disrupted by incubating them in 10 mM Tris-HCl (pH 7.5), 1 mM EDTA, 1 M NaCl, and 2 M β-mercaptoethanol at 75°C for 3 hr on the basis of a previously described protocol (Jenne and Famulok, 1999). Free DNA fragments were purified with a QIAquick PCR Purification Kit (QIAGEN). To determine the efficiency of $KMnO_4$ and nuclease treatment, biotinylation, and purification, we measured the DNA concentration for each concentration of mung bean nuclease used and for each sample (nuclease-untreated DNA; nuclease-untreated, KMnO4-treated DNA; mung bean nuclease-treated DNA; and KMnO4- and mung bean nuclease-treated DNA).

Experiments that showed the relative DNA recoveries 0-0-1-20 (a-b-c-d) were chosen for additional processing. In these experiments, the KMnO4-treated DNA samples yielded a 3–5 kb average size of fragments after nuclease digestion.

Library Construction

To remove biotinylated tails from DNA, sample d from above were incubated with 30 U of S1 nuclease (Fermentas) in 100 μl of recommended buffer for 30 min at 37°C. DNA was purified with a QIAquick PCR Purification Kit (QIAGEN).

ACCESSION NUMBERS

PolII-seq data were deposited in the Gene Expression Omnibus under accession number GSE24178, RNA-seq data under accession number GSE21630, and ssDNA-seq data under accession number SRA072844.

SUPPLEMENTAL INFORMATION

Supplemental Information includes Extended Experimental Procedures, six figures, and one table and can be found with this article online at http://dx.doi.org/10.1016/j.cell.2013.04.033.

ACKNOWLEDGMENTS

We thank G. Gutierrez for technical assistance with the genome analyzer; J. Simone and J. Lay for bone marrow sorts; J. Qian and K. Zaal for the B cell confocal micrographs; and C. Benham for SIDD mapping. We thank the Casellas and Levens lab members for critically reading the manuscript. We also thank A. Hoofring from the National Institutes of Health (NIH) Medical Arts for designing the pictures shown in Figure 6D. This work was supported in part by the Intramural Research Program of National Institute of Arthritis and Musculoskeletal and Skin Diseases (NAIMS), the National Cancer Institute (Center for Cancer Research), and the National Library of Medicine of the NIH. This study utilized the high-performance computational capabilities of the Helix Systems at the NIH (http://helix.nih.gov). All animal experiments were performed according to the NIH guidelines for laboratory animals and were approved by the Scientific Committee of the NIAMS Animal Facilities. For questions regarding computational analysis, please contact T.M.P. (przytyck@ncbi.nlm.nih.gov).

Received: May 25, 2012
Revised: January 31, 2013
Accepted: April 4, 2013
Published: May 23, 2013

REFERENCES

Assfalg, R., Lebedev, A., Gonzalez, O.G., Schelling, A., Koch, S., and Iben, S. (2012). TFIIH is an elongation factor of RNA polymerase I. Nucleic Acids Res. *40*, 650–659.

Barlow, J.H., Faryabi, R.B., Callén, E., Wong, N., Malhowski, A., Chen, H.T., Gutierrez-Cruz, G., Sun, H.W., McKinnon, P., Wright, G.W., et al. (2013). Identification of early replicating fragile sites that contribute to genome instability. Cell *152*, 620–632.

Benham, C.J., and Bi, C. (2004). The analysis of stress-induced duplex destabilization in long genomic DNA sequences. J. Comput. Biol. *11*, 519–543.

Bentley, D.L., and Groudine, M. (1986). A block to elongation is largely responsible for decreased transcription of c-myc in differentiated HL60 cells. Nature *321*, 702–706.

Bernstein, B.E., Mikkelsen, T.S., Xie, X., Kamal, M., Huebert, D.J., Cuff, J., Fry, B., Meissner, A., Wernig, M., Plath, K., et al. (2006). A bivalent chromatin structure marks key developmental genes in embryonic stem cells. Cell *125*, 315–326.

Calvo, K.R., Dabir, B., Kovach, A., Devor, C., Bandle, R., Bond, A., Shih, J.H., and Jaffe, E.S. (2008). IL-4 protein expression and basal activation of Erk in vivo in follicular lymphoma. Blood *112*, 3818–3826.

Cer, R.Z., Bruce, K.H., Mudunuri, U.S., Yi, M., Volfovsky, N., Luke, B.T., Bacolla, A., Collins, J.R., and Stephens, R.M. (2011). Non-B DB: a database of predicted non-B DNA-forming motifs in mammalian genomes. Nucleic Acids Res. *39*(Database issue), D383–D391.

Core, L.J., Waterfall, J.J., and Lis, J.T. (2008). Nascent RNA sequencing reveals widespread pausing and divergent initiation at human promoters. Science *322*, 1845–1848.

de Boer, J., de Wit, J., van Steeg, H., Berg, R.J., Morreau, H., Visser, P., Lehmann, A.R., Duran, M., Hoeijmakers, J.H., and Weeda, G. (1998). A mouse model for the basal transcription/DNA repair syndrome trichothiodystrophy. Mol. Cell *1*, 981–990.

Di Virgilio, M., Callen, E., Yamane, A., Zhang, B., Jankovic, M., Gitlin, A.D., Feldhahn, N., Resch, W., Oliveira, T.Y., Chait, B.T., et al. (2013). Rif1 Prevents Resection of DNA Breaks and Promotes Immunoglobulin Class Switching. Science.

Du, Z., Zhao, Y., and Li, N. (2008). Genome-wide analysis reveals regulatory role of G4 DNA in gene transcription. Genome Res. *18*, 233–241.

Dvir, A. (2002). Promoter escape by RNA polymerase II. Biochim. Biophys. Acta *1577*, 208–223.

Feaver, W.J., Svejstrup, J.Q., Henry, N.L., and Kornberg, R.D. (1994). Relationship of CDK-activating kinase and RNA polymerase II CTD kinase TFIIH/TFIIK. Cell *79*, 1103–1109.

Fisher, R.P. (2005). Secrets of a double agent: CDK7 in cell-cycle control and transcription. J. Cell Sci. *118*, 5171–5180.

Fuda, N.J., Ardehali, M.B., and Lis, J.T. (2009). Defining mechanisms that regulate RNA polymerase II transcription in vivo. Nature *461*, 186–192.

Giglia-Mari, G., Theil, A.F., Mari, P.O., Mourgues, S., Nonnekens, J., Andrieux, L.O., de Wit, J., Miquel, C., Wijgers, N., Maas, A., et al. (2009). Differentiation driven changes in the dynamic organization of Basal transcription initiation. PLoS Biol. *7*, e1000220.

Gilmour, D.S., and Lis, J.T. (1986). RNA polymerase II interacts with the promoter region of the noninduced hsp70 gene in Drosophila melanogaster cells. Mol. Cell. Biol. *6*, 3984–3989.

Goodrich, J.A., and Tjian, R. (1994). Transcription factors IIE and IIH and ATP hydrolysis direct promoter clearance by RNA polymerase II. Cell *77*, 145–156.

Guenther, M.G., Levine, S.S., Boyer, L.A., Jaenisch, R., and Young, R.A. (2007). A chromatin landmark and transcription initiation at most promoters in human cells. Cell *130*, 77–88.

Guzmán, E., and Lis, J.T. (1999). Transcription factor TFIIH is required for promoter melting in vivo. Mol. Cell. Biol. *19*, 5652–5658.

Hakim, O., Resch, W., Yamane, A., Klein, I., Kieffer-Kwon, K.-R., Jankovic, M., Oliveira, T., Bothmer, A., Voss, T.C., Ansarah-Sobrinho, C., et al. (2012). DNA damage defines sites of recurrent chromosomal translocations in B lymphocytes. Nature *484*, 69–74.

Heintzman, N.D., Stuart, R.K., Hon, G., Fu, Y., Ching, C.W., Hawkins, R.D., Barrera, L.O., Van Calcar, S., Qu, C., Ching, K.A., et al. (2007). Distinct and predictive chromatin signatures of transcriptional promoters and enhancers in the human genome. Nat. Genet. *39*, 311–318.

Holstege, F.C., van der Vliet, P.C., and Timmers, H.T. (1996). Opening of an RNA polymerase II promoter occurs in two distinct steps and requires the basal transcription factors IIE and IIH. EMBO J. *15*, 1666–1677.

Holstege, F.C., Fiedler, U., and Timmers, H.T. (1997). Three transitions in the RNA polymerase II transcription complex during initiation. EMBO J. *16*, 7468–7480.

Jaehning, J.A., Stewart, C.C., and Roeder, R.G. (1975). DNA-dependent RNA polymerase levels during the response of human peripheral lymphocytes to phytohemagglutinin. Cell *4*, 51–57.

Jenne, A., and Famulok, M. (1999). Disruption of the streptavidin interaction with biotinylated nucleic acid probes by 2-mercaptoethanol. Biotechniques *26*, 249–252, 254.

Keller, W. (1975). Determination of the number of superhelical turns in simian virus 40 DNA by gel electrophoresis. Proc. Natl. Acad. Sci. USA *72*, 4876–4880.

Khil, P.P., Smagulova, F., Brick, K.M., Camerini-Otero, R.D., and Petukhova, G.V. (2012). Sensitive mapping of recombination hotspots using sequencing-based detection of ssDNA. Genome Res. *22*, 957–965.

Kim, T.K., Ebright, R.H., and Reinberg, D. (2000). Mechanism of ATP-dependent promoter melting by transcription factor IIH. Science *288*, 1418–1422.

Kim, T.H., Barrera, L.O., Zheng, M., Qu, C., Singer, M.A., Richmond, T.A., Wu, Y., Green, R.D., and Ren, B. (2005). A high-resolution map of active promoters in the human genome. Nature *436*, 876–880.

Kim, T.K., Hemberg, M., Gray, J.M., Costa, A.M., Bear, D.M., Wu, J., Harmin, D.A., Laptewicz, M., Barbara-Haley, K., Kuersten, S., et al. (2010). Widespread transcription at neuronal activity-regulated enhancers. Nature *465*, 182–187.

Klemsz, M.J., Justement, L.B., Palmer, E., and Cambier, J.C. (1989). Induction of c-fos and c-myc expression during B cell activation by IL-4 and immunoglobulin binding ligands. J. Immunol. *143*, 1032–1039.

Kouzine, F., and Levens, D. (2007). Supercoil-driven DNA structures regulate genetic transactions. Front. Biosci. *12*, 4409–4423.

Kouzine, F., Liu, J., Sanford, S., Chung, H.J., and Levens, D. (2004). The dynamic response of upstream DNA to transcription-generated torsional stress. Nat. Struct. Mol. Biol. *11*, 1092–1100.

Kouzine, F., Sanford, S., Elisha-Feil, Z., and Levens, D. (2008). The functional response of upstream DNA to dynamic supercoiling in vivo. Nat. Struct. Mol. Biol. *15*, 146–154.

Kuchen, S., Resch, W., Yamane, A., Kuo, N., Li, Z., Chakraborty, T., Wei, L., Laurence, A., Yasuda, T., Peng, S., et al. (2010). Regulation of microRNA expression and abundance during lymphopoiesis. Immunity *32*, 828–839.

Lee, T.I., and Young, R.A. (2000). Transcription of eukaryotic protein-coding genes. Annu. Rev. Genet. *34*, 77–137.

Lee, T.I., Jenner, R.G., Boyer, L.A., Guenther, M.G., Levine, S.S., Kumar, R.M., Chevalier, B., Johnstone, S.E., Cole, M.F., Isono, K., et al. (2006). Control of developmental regulators by Polycomb in human embryonic stem cells. Cell *125*, 301–313.

Liao, S.M., Zhang, J., Jeffery, D.A., Koleske, A.J., Thompson, C.M., Chao, D.M., Viljoen, M., van Vuuren, H.J., and Young, R.A. (1995). A kinase-cyclin pair in the RNA polymerase II holoenzyme. Nature *374*, 193–196.

Lin, C.Y., Lovén, J., Rahl, P.B., Paranal, R.M., Burge, C.B., Bradner, J.E., Lee, T.I., and Young, R.A. (2012). Transcriptional amplification in tumor cells with elevated c-Myc. Cell *151*, 56–67.

Liu, M., Tolstorukov, M., Zhurkin, V., Garges, S., and Adhya, S. (2004). A mutant spacer sequence between -35 and -10 elements makes the Plac promoter hyperactive and cAMP receptor protein-independent. Proc. Natl. Acad. Sci. USA *101*, 6911–6916.

Lovén, J., Orlando, D.A., Sigova, A.A., Lin, C.Y., Rahl, P.B., Burge, C.B., Levens, D.L., Lee, T.I., and Young, R.A. (2012). Revisiting global gene expression analysis. Cell *151*, 476–482.

Lutz, R., Lozinski, T., Ellinger, T., and Bujard, H. (2001). Dissecting the functional program of Escherichia coli promoters: the combined mode of action of Lac repressor and AraC activator. Nucleic Acids Res. *29*, 3873–3881.

Margaritis, T., and Holstege, F.C. (2008). Poised RNA polymerase II gives pause for thought. Cell *133*, 581–584.

Melchers, F., and Andersson, J. (1984). B cell activation: three steps and their variations. Cell *37*, 713–720.

Mirkovitch, J., and Darnell, J.E., Jr. (1992). Mapping of RNA polymerase on mammalian genes in cells and nuclei. Mol. Biol. Cell *3*, 1085–1094.

Muse, G.W., Gilchrist, D.A., Nechaev, S., Shah, R., Parker, J.S., Grissom, S.F., Zeitlinger, J., and Adelman, K. (2007). RNA polymerase is poised for activation across the genome. Nat. Genet. *39*, 1507–1511.

Nie, Z., Hu, G., Wei, G., Cui, K., Yamane, A., Resch, W., Wang, R., Green, D.R., Tessarollo, L., Casellas, R., et al. (2012). c-Myc is a universal amplifier of expressed genes in lymphocytes and embryonic stem cells. Cell *151*, 68–79.

Ohkuma, Y., Hashimoto, S., Wang, C.K., Horikoshi, M., and Roeder, R.G. (1995). Analysis of the role of TFIIE in basal transcription and TFIIH-mediated carboxy-terminal domain phosphorylation through structure-function studies of TFIIE-alpha. Mol. Cell. Biol. *15*, 4856–4866.

Orphanides, G., and Reinberg, D. (2000). RNA polymerase II elongation through chromatin. Nature *407*, 471–475.

Parvin, J.D., and Sharp, P.A. (1993). DNA topology and a minimal set of basal factors for transcription by RNA polymerase II. Cell *73*, 533–540.

Pogo, B.G., Allfrey, V.G., and Mirsky, A.E. (1966). RNA synthesis and histone acetylation during the course of gene activation in lymphocytes. Proc. Natl. Acad. Sci. USA *55*, 805–812.

Pogo, B.G., Allfrey, V.G., and Mirsky, A.E. (1967). The effect of phytohemagglutinin on ribonucleic acid synthesis and histone acetylation in equine leukocytes. J. Cell Biol. *35*, 477–482.

Ptashne, M., and Gann, A. (1997). Transcriptional activation by recruitment. Nature *386*, 569–577.

Radonjic, M., Andrau, J.C., Lijnzaad, P., Kemmeren, P., Kockelkorn, T.T., van Leenen, D., van Berkum, N.L., and Holstege, F.C. (2005). Genome-wide analyses reveal RNA polymerase II located upstream of genes poised for rapid response upon S. cerevisiae stationary phase exit. Mol. Cell *18*, 171–183.

Raghavan, S.C., and Lieber, M.R. (2006). DNA structures at chromosomal translocation sites. Bioessays *28*, 480–494.

Rahl, P.B., Lin, C.Y., Seila, A.C., Flynn, R.A., McCuine, S., Burge, C.B., Sharp, P.A., and Young, R.A. (2010). c-Myc regulates transcriptional pause release. Cell *141*, 432–445.

Rajewsky, K. (1996). Clonal selection and learning in the antibody system. Nature *381*, 751–758.

Rawlings, J.S., Gatzka, M., Thomas, P.G., and Ihle, J.N. (2011). Chromatin condensation via the condensin II complex is required for peripheral T-cell quiescence. EMBO J. *30*, 263–276.

Roeder, R.G. (2005). Transcriptional regulation and the role of diverse coactivators in animal cells. FEBS Lett. *579*, 909–915.

Sawai, M., Takase, K., Teraoka, H., and Tsukada, K. (1990). Reversible G1 arrest in the cell cycle of human lymphoid cell lines by dimethyl sulfoxide. Exp. Cell Res. *187*, 4–10.

Seila, A.C., Core, L.J., Lis, J.T., and Sharp, P.A. (2009). Divergent transcription: a new feature of active promoters. Cell Cycle *8*, 2557–2564.

Shapiro-Shelef, M., and Calame, K. (2005). Regulation of plasma-cell development. Nat. Rev. Immunol. *5*, 230–242.

Shklover, J., Weisman-Shomer, P., Yafe, A., and Fry, M. (2010). Quadruplex structures of muscle gene promoter sequences enhance in vivo MyoD-dependent gene expression. Nucleic Acids Res. *38*, 2369–2377.

Sprent, J. (1993). Lifespans of naive, memory and effector lymphocytes. Curr. Opin. Immunol. *5*, 433–438.

Sterner, D.E., Lee, J.M., Hardin, S.E., and Greenleaf, A.L. (1995). The yeast carboxyl-terminal repeat domain kinase CTDK-I is a divergent cyclin-cyclin-dependent kinase complex. Mol. Cell. Biol. *15*, 5716–5724.

Tu, C.P., and Cohen, S.N. (1980). 3′-end labeling of DNA with [alpha-32P]cordycepin-5′-triphosphate. Gene *10*, 177–183.

Vermeulen, W., van Vuuren, A.J., Chipoulet, M., Schaeffer, L., Appeldoorn, E., Weeda, G., Jaspers, N.G., Priestley, A., Arlett, C.F., Lehmann, A.R., et al. (1994). Three unusual repair deficiencies associated with transcription factor BTF2(TFIIH): evidence for the existence of a transcription syndrome. Cold Spring Harb. Symp. Quant. Biol. *59*, 317–329.

Vermeulen, W., Rademakers, S., Jaspers, N.G., Appeldoorn, E., Raams, A., Klein, B., Kleijer, W.J., Hansen, L.K., and Hoeijmakers, J.H. (2001). A temperature-sensitive disorder in basal transcription and DNA repair in humans. Nat. Genet. *27*, 299–303.

Wang, Z., Zang, C., Rosenfeld, J.A., Schones, D.E., Barski, A., Cuddapah, S., Cui, K., Roh, T.Y., Peng, W., Zhang, M.Q., and Zhao, K. (2008). Combinatorial patterns of histone acetylations and methylations in the human genome. Nat. Genet. *40*, 897–903.

Yafe, A., Shklover, J., Weisman-Shomer, P., Bengal, E., and Fry, M. (2008). Differential binding of quadruplex structures of muscle-specific genes regulatory sequences by MyoD, MRF4 and myogenin. Nucleic Acids Res. *36*, 3916–3925.

Yamane, A., Resch, W., Kuo, N., Kuchen, S., Li, Z., Sun, H.W., Robbiani, D.F., McBride, K., Nussenzweig, M.C., and Casellas, R. (2011). Deep-sequencing identification of the genomic targets of the cytidine deaminase AID and its cofactor RPA in B lymphocytes. Nat. Immunol. *12*, 62–69.

Yamane, A., Robbiani, D.F., Resch, W., Bothmer, A., Nakahashi, H., Oliveira, T., Rommel, P.C., Brown, E.J., Nussenzweig, A., Nussenzweig, M.C., and Casellas, R. (2013). RPA accumulation during class switch recombination represents 5′-3′ DNA-end resection during the S-G2/M phase of the cell cycle. Cell Rep *3*, 138–147.

Zeitlinger, J., Stark, A., Kellis, M., Hong, J.W., Nechaev, S., Adelman, K., Levine, M., and Young, R.A. (2007). RNA polymerase stalling at developmental control genes in the Drosophila melanogaster embryo. Nat. Genet. *39*, 1512–1516.

Zhou, Z.-X., Zhang, M.-J., Peng, X., Takayama, Y., Xu, X.-Y., Huang, L.-Z., and Du, L.-L. (2013). Mapping genomic hotspots of DNA damage by a single-strand-DNA-compatible and strand-specific ChIP-seq method. Genome Res. *23*, 705–715.